Demonstration of a Mid-Infrared Carbon Monoxide Sensor

by

Nicholas Fitzgerald Herrick-Kaiser

A Thesis Submitted to the Graduate
Faculty of Rensselaer Polytechnic Institute
in Partial Fulfillment of the
Requirements for the degree of
MASTER OF SCIENCE
Major Subject: Aeronautical Engineering

Approved:

_____
Matthew Oehlschlaeger, Thesis Adviser

Rensselaer Polytechnic Institute
Troy, New York

April, 2008
(For Graduation May, 2008)

CONTENTS

LIST OF FIGURES

ACKNOWLEDGMENT

Without the help and support of many people this thesis would not have been possible. Thank you to my advisor Matt for even making graduate school a possibility for me, and for not only making it a highly educational experience, but also an enjoyable one. Also, thank you to the lab guys for making it a fun place to work. I must also thank my roommates who are like my family away from home to me. Of course, without the support and love of my family, none of my educational goals may have ever come to be, and I am forever thankful for that.

ABSTRACT

Initial stages in the development of a carbon monoxide diagnostic are completed. This diagnostic is unique in that it utilizes mid-infrared radiation generated by a quantum cascade laser to perform absorption spectroscopy. Past absorption spectroscopy systems have utilized the near-infrared; the mid-infrared region contains significantly stronger absorption features than the near-infrared, these stronger features can be harnessed to develop a diagnostic which is far more sensitive. The strong sensitivity of mid-infrared spectroscopy and small size of quantum cascade lasers enables the goal of a small, non-intrusive, highly sensitive diagnostic which can be used for process monitoring in various combustion and energy systems.

A brief review of past work with quantum cascade lasers and basic absorption spectroscopy fundamentals are presented. Development of the diagnostic system is described in detail, including the principles behind quantum cascade lasers. Laser functionality is validated and initial qualitative measurements are made; the R(11) carbon monoxide absorbance line is observed and identified. Significant future work is required for accurate qualitative measurements on combustion and energy systems; suggestions for future work are given.

1. INTRODUCTION

1.1 Motivation

Many modern energy systems rely on the ability to monitor various processes in real time to allow control. Specifically, the areas of combustion, fuel cells, and propulsion are becoming increasingly dependent on real-time accurate sensors to improve efficiency and performance in this time of increasing energy demand and cost. Gas phase sensing is important to these areas as gas concentration and temperature data is desired at several stations throughout these systems. Gas phase concentration measurements can be acquired using several methods, including gas chromatography, FTIR, solid-solid state techniques, and laser absorption spectroscopy.

Laser absorption spectroscopy has been utilized successfully in the measurement of gas concentration for some time. This method has been of particular interest because it is non-intrusive, generally faster, more sensitive and more accurate than the alternatives. While initially the main application interest is a laboratory setting, a long-term goal is the development of laser sensors for industrial applications, particularly in the areas of combustion, fuel cell power generation and propulsion devices.

Past work has largely utilized laser/sensors which use the ro-vibrational overtone bands in the near-IR. Lasers which operate in this near-IR range are well developed and commercially available due to their significant use by the telecommunications industry. While the near-IR has been used successfully in the past, the mid-IR contains fundamental ro-vibrational bands which have significantly higher absorption strengths than those in the near-IR. The stronger absorption lines found in the mid-IR enable concentration measurements which are far more sensitive than those previously possible using near-IR.

Mid-IR spectroscopy has been largely limited to this point by the difficulties of generating mid-IR laser radiation with properties needed for laser spectroscopy (single mode and sufficient power). Past use of the mid-IR absorption features has required the use of less convenient (compared to the cheap, durable near-IR systems) low-power multimode cryogenically cooled lead-salt diode lasers, fixed-wavelength HeNe lasers, or CO and CO_2 lasers. More recently, there has been a great deal of development in

quantum cascade lasers; these devices are becoming significantly more convenient and affordable, in part, overcoming a major barrier to mid-IR spectroscopy.

The mid-IR absorption bands provide an enormous (several orders of magnitude) increase in sensitivity over the near-IR counterpart; **Figure 1.1** illustrates absorptions for CO, CO_2, and H_2O over the IR spectrum (both near and mid IR).

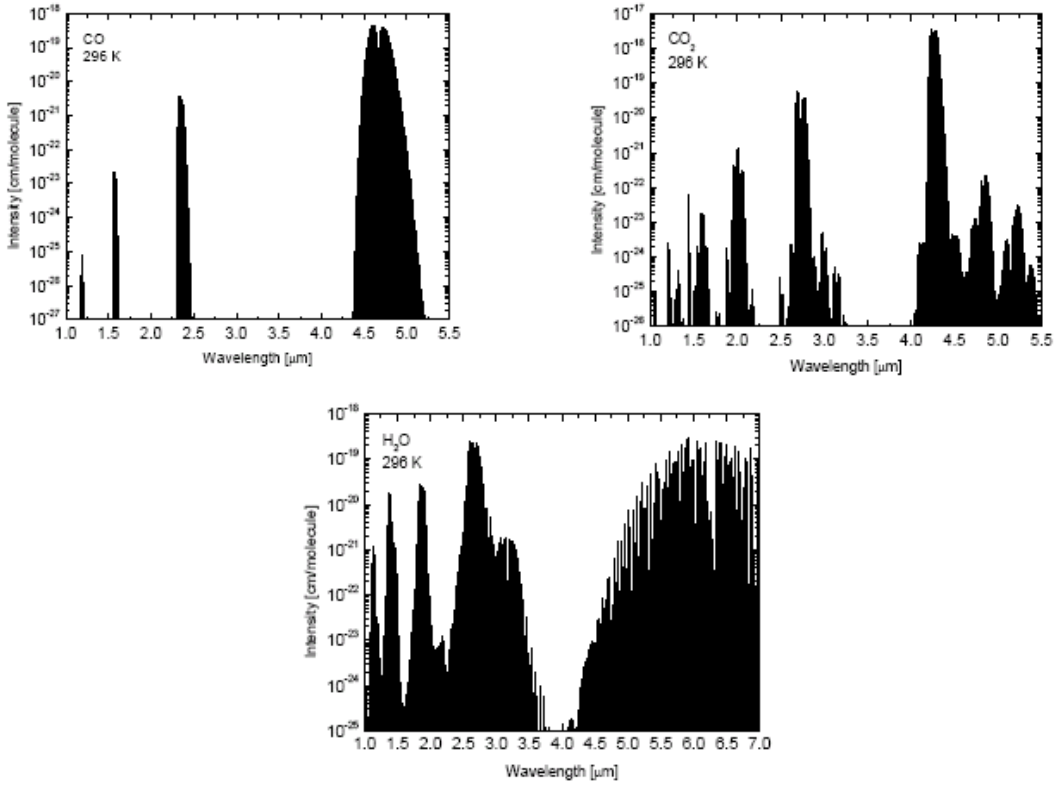

Figure 1.1 Absorption strengths for CO, CO_2, and H_2O at 296 K, simulated using HITRAN 2004 [1].

Clearly the mid-IR bands (4 – 7 μm) show much greater line strengths than the features located in the near IR (1 – 3.5 μm). Not only does this allow measurements which are unattainable with current equipment, but additionally the use of significantly shorter pathlengths is made possible; these small pathlengths are essential to the development of miniature sensors for use in devices with much smaller pathlengths and miniature probes which can be placed into systems of interest [1].

1.2 Previous Work in mid-IR Spectroscopy

Advancement of quantum cascade lasers has been relatively recent; from initial development in 1994, to the first gas measurements in 1998, and more recently the evolution into distributed feedback quantum cascade lasers (DFB-QCLs). These DFB-QCLs are capable of producing the narrow linewidth, single-frequency, high power, tunable mid-IR radiation needed for mid-IR spectroscopy.

These DFB-QCLs are currently available in two modes: pulsed and continuous wave. Currently, pulsed DFB-QCLs offer a much wider array of wavelengths than the alternative continuous wave. Most of these units operate around room temperature, relying solely on thermoelectric cooling, while some require more elaborate cryogenic cooling systems. Several groups have demonstrated these devices inside and outside the laboratory. Tittel and co-workers have successfully measured a range of gases in laboratory and natural environments; experiments have included atmospheric monitoring, volcano monitoring, and human breath analysis, to name a few. Traditional scanned-wavelength technique along with several sensitivity enhancing methods (integrated cavity output spectroscopy and cavity ringdown spectroscopy) were used in these experiments; yielded results were very sensitive, on the ppb level [2-4].

Additional work with QCLs includes but is not limited to the following: measurement of NO in human breath by Roller et al. [5], precise measurement of NH_3 to the ppb level using cavity ringdown spectroscopy in a laboratory cell by Paldus et al. [6], the measurement of NH_3, C_2H_4, and NO in cigarette smoke by Shi et al. [7], use of wavelength modulation techniques by Namjou et al. to measure CH_4 and N_2O in a gas cell [8]. Wehe et al. have made the first advances into using QCLs for combustion applications, with use of QCLs to measure CO and NO in a laboratory cell [9].

1.3 Statement of Work

Because of the very limited use of QCLs and mid-IR spectroscopy, the first and primary objective was to construct a system to measure simple species concentration, and eventually temperature. For this thesis, the measurement of CO is of interest.

Concentration and temperature measurement can be achieved through several different methods including fixed-wavelength direct absorption, scanned-wavelength direct absorption, and wavelength modulation spectroscopy (WMS) with harmonic frequency detection; these three options are illustrated in Figure 1.2, below. While each method has advantages and disadvantages, this thesis will only utilize scanned wavelength spectroscopy for its simplicity. However, the future of this project will likely see the use the wavelength modulation to attain more sensitive measurements.

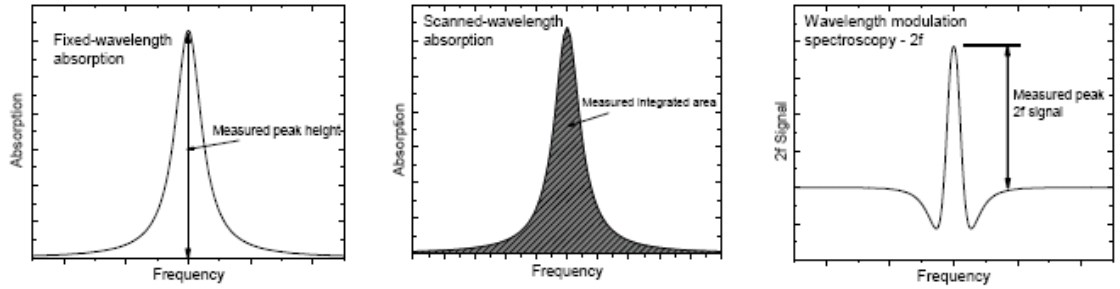

Figure 1.2 - Fixed-wavelength absorption, scanned-wavelength absorption, and WMS, respectively.

Fixed-wavelength direct absorption measures concentration using the peak absorption magnitude, scanned-wavelength integrates the absorption profile to determine concentration, while WMS excites and measures harmonic frequencies by modulating the laser frequency.

The sensor setup utilizes a thermoelectrically cooled pulsed DFB-QCL from Alpes Lasers [10]. Both fixed-wavelength and scanned-wavelength direction absorption techniques are used, using quasi-cw operation via driving the QCL with short injection current pulses (5-20 ns) at high repetition rates (~1 MHz). By adding a varying subthreshold current, via a bias-tee, which is super imposed on the short current pulses the wavelength can be varied rapidly; this rapid variation in wavelength is achieved by the rapid heating and cooling the active region of the QCL undergoes during the variation of the subthreshold current. Changing operating temperature, via a thermoelectric Peltier cooler, is effective for slow variation in wavelength.

2. ABSORPTION THEORY

2.1 Beer-Lambert Law

The Beer-Lambert law is the governing principle behind absorption spectroscopy; it relates the fraction of non-absorbed (transmitted) radiation to the path length L and spectral absorption coefficient k_v.

$$T_v = \frac{I}{I_0} = \exp(k_v L)$$

Spectral absorption coefficient is a function of the species being measured; the species' fundamental lineshape, linestrength, concentration, as well as temperature, pressure, and gas composition. This coefficient is expanded in a number of ways, depending on the literature; a common notation expands it into the above mentioned parameters, as follows:

$$k_v = -S_i \phi P X_j$$

Where S_i is the linestrength for the ith transition, ϕ is the spectral lineshape, P is total pressure, and X_j is the concentration of the jth species. This relation is sometimes expressed in a more complete form which accounts for overlapping transitions as well as a multiple-species environment, as shown here for K species and N_j overlapping transitions:

$$k_v = P \sum_{j=1}^{K} X_j \sum_{i=1}^{N_j} S_{i,j}(T) \phi_{i,j}$$

2.2 Linestrength

Each absorption transition has a linestrength which is dependent on the Boltzmann fraction, as well as the probability of the transition, which is a function of the spectral characteristics of the specific molecule's transition. As a result of the Boltzmann fraction dependence, the linestrength is a function of temperature.

If the reference linestrength for a given transition, $S_i(T_O)$, is known, the linestrength at a given temperature, *T*, can be found using the following relation.

$$S_i(T) = S_i(T_0)\frac{Q(T_0)}{Q(T)}\left(\frac{T_0}{T}\right)\exp\left[-\frac{hcE_i^{"}}{k}\left(\frac{1}{T}-\frac{1}{T_0}\right)\right]\left[1-\exp\left(\frac{-hcv_{0,i}}{kT}\right)\right]\left[1-\exp\left(\frac{-hcv_{0,i}}{kT_0}\right)\right]^{-1}$$

2.3 Lineshape

Lineshape refers to the variance in absorption intensity with changing frequency. At each transition (line), absorption is not discrete, rather there is a distribution centered at the fundamental frequency or linecenter.

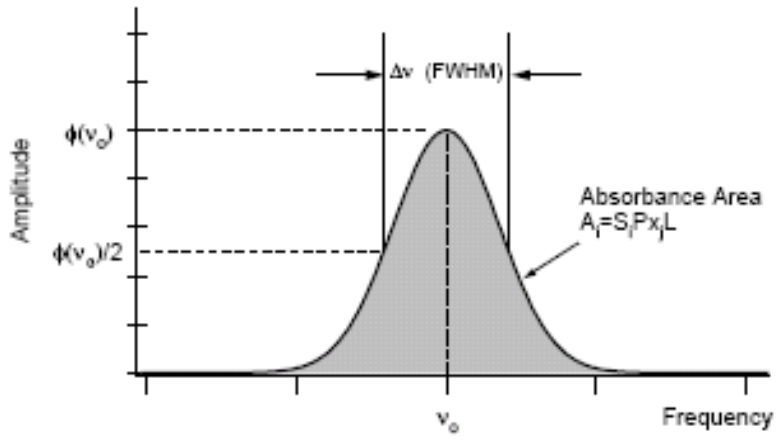

Figure 2.1 – Sample lineshape distribution over frequency [11].

Lineshape is normalized such that integration over frequency will result in a value of one.

$$\int_{-\infty}^{+\infty}\phi dv = 1$$

Linewidth is a measurement of the lineshape, usually defined by the width at half the maximum amplitude (absorbance) of the feature (the full width at half maximum value, FWHM). Broadening of the linewidth can occur via several mechanisms, the main

contributors being Doppler and collisional broadening, with natural broadening and Dicke narrowing (however, these are generally negligible).

2.3.1 Doppler Broadening

When a molecule being sampled has velocity in the same direction as light passing through, the lineshape is altered; this alteration is known as a Doppler shift. Molecules are in constant random motion; according to statistical mechanics the motion is described by a Maxwellian velocity distribution function. If molecules are divided into velocity classes (groupings of molecules with velocity in the same direction), the distribution indicates how many molecules are in each class. Because each class has a different velocity component in the direction of light passing through, a different Doppler shift will exist for each class. The classes are arranged in a Gaussian distribution, which defines the lineshape function as follows:

$$\phi_D = \frac{2}{\Delta\nu_D}\left(\frac{\ln 2}{\pi}\right)^{1/2} \exp\left\{-4\ln 2\left(\frac{\nu-\nu_0}{\Delta\nu_D}\right)^2\right\}$$

where $\Delta\nu_D$ is the Doppler width (full width at half maximum, FWHM) of the lineshape; defined by:

$$\Delta\nu_D = \nu_0\sqrt{\frac{8kT\ln 2}{mc^2}} = 7.1623x10^{-7}\nu_0\sqrt{\frac{T}{M}}$$

where ν_0 is the linecenter, T is the temperature, and M the molecular weight of the species of interest.

Doppler lineshape peak height at the linecenter is

$$\phi_D(\nu_0) = \frac{2}{\Delta\nu_D}\sqrt{\frac{\ln 2}{\pi}}$$

2.3.2 Collisional Broadening

The constant random motion of molecules in a gas inherently leads to collisions. When collisions occur, the energy states of the molecules involved change, potentially

changing the energy level of the molecule. As the number of collisions increases, the shorter the energy level lifetime of the molecules; the Heisenberg uncertainty principle infers that the shorter the energy level lifetime of a molecule the greater the uncertainty of its energy level. As uncertainty in the energy levels of molecules in the gas increases, the lineshape broadens, hence collisional broadening.

A Lorenzian function describes the lineshape when collisional broadening is the primary broadening mechanism; this function is defined as:

$$\phi_C(\nu) = \frac{1}{2\pi} \frac{\Delta\nu_C}{(\nu - \nu_0)^2 + \left(\frac{\Delta\nu_C}{2}\right)^2}$$

At the linecenter, the Lorenzian peak is

$$\phi_C(\nu_0) = \frac{2}{\pi\Delta\nu_C}$$

As pressure increases, the number density of the gas is raised, increasing the likelihood of collisions; at constant temperature, pressure is directly proportional to the collisional broadening.

$$\Delta\nu_C = P\sum_j X_j \gamma_j$$

Where X_j is the mole fraction of the molecule of interest, and γ_j is its' inherent collisional broadening coefficient. Two types of collisions occur; self broadening is a result of molecules of the same species colliding, while foreign-gas broadening occurs when molecules of two different species collide. The two different collision types have their own collisional broadening coefficients, depending on the species involved.

Collisional broadening is also temperature dependent; this dependence is reflected in the broadening coefficient, which is a function of the aforementioned:

$$\gamma_j(T) = \gamma_j(T_0)\left(\frac{T_0}{T}\right)^{n_j}$$

Where T_0 is the reference temperature, and n_j is the temperature dependence exponent (usually about 0.5).

2.3.3 Voigt Profiles

The aforementioned Doppler and collisional lineshape definitions are only valid when one of the two is the dominant broadening mechanism and the other is negligible in comparison. In many cases, both are too significant to be neglected, meaning neither Doppler or collisional lineshape functions are valid. Rather, a convolution combining both is used, this is known as the Voigt function:

$$\phi_V(\nu) = \int_{-\infty}^{+\infty} \phi_D(u)\phi_C(\nu - u)du$$

This essentially states that each velocity class (of the Gaussian/Doppler distribution) is collisionally broadened, forming the convolution of the two mechanisms.

Three major parameters are defined in the derivation of the common Voigt profile. The relative significance of Doppler and collisional broadening is defined by the Voigt parameter, a

$$a = \frac{\sqrt{\ln 2}\Delta\nu_C}{\Delta\nu_D}$$

The non-dimensional line position parameter, w, is a measure of the distance from the line center, and is defined as:

$$w = \frac{2\sqrt{\ln 2}(\nu - \nu_0)}{\Delta\nu_D}$$

Finally, the integral variable, y, is defined as

$$y = \frac{2\sqrt{\ln 2u}}{\Delta\nu_D}$$

Use of these parameters in conjunction with the linecenter Gaussian magnitude results in the common form of the Voigt profile

$$\phi_V(\nu) = \frac{2}{\Delta\nu_D}\sqrt{\frac{\ln 2}{\pi}}\frac{a}{\pi}\int_{-\infty}^{+\infty}\frac{\exp(-y^2)}{a^2 + (w-y)^2}dy = \phi_D(\nu)\frac{a}{\pi}\int_{-\infty}^{+\infty}\frac{\exp(-y^2)}{a^2 + (w-y)^2}dy$$

Because usually neither Doppler or collisional broadening are able to be neglected, the Voigt profile is generally the basis lineshape profile for absorption spectroscopy. However, the form stated above is difficult to work with; several numerical approximations have been developed as a result.

The FWHM of the Voigt lineshape can be approximated as

$$\Delta\nu_V = 0.5346\Delta\nu_C + \sqrt{0.2166\Delta\nu_C{}^2 + \Delta\nu_D{}^2}$$

Additionally, the peak height can be estimated by

$$\phi_V(\nu_0) = \left[\left(\frac{\beta}{\gamma_{ED}\sqrt{\pi}}\right) + \left(\frac{1-\beta}{\pi\gamma_C}\right)\right]$$

where

$$\beta = \left(\frac{\gamma_{ED}}{(\gamma_C + \gamma_{ED})}\right) \text{ and } \gamma_{ED} = \frac{\gamma_D}{\sqrt{\ln 2}}$$

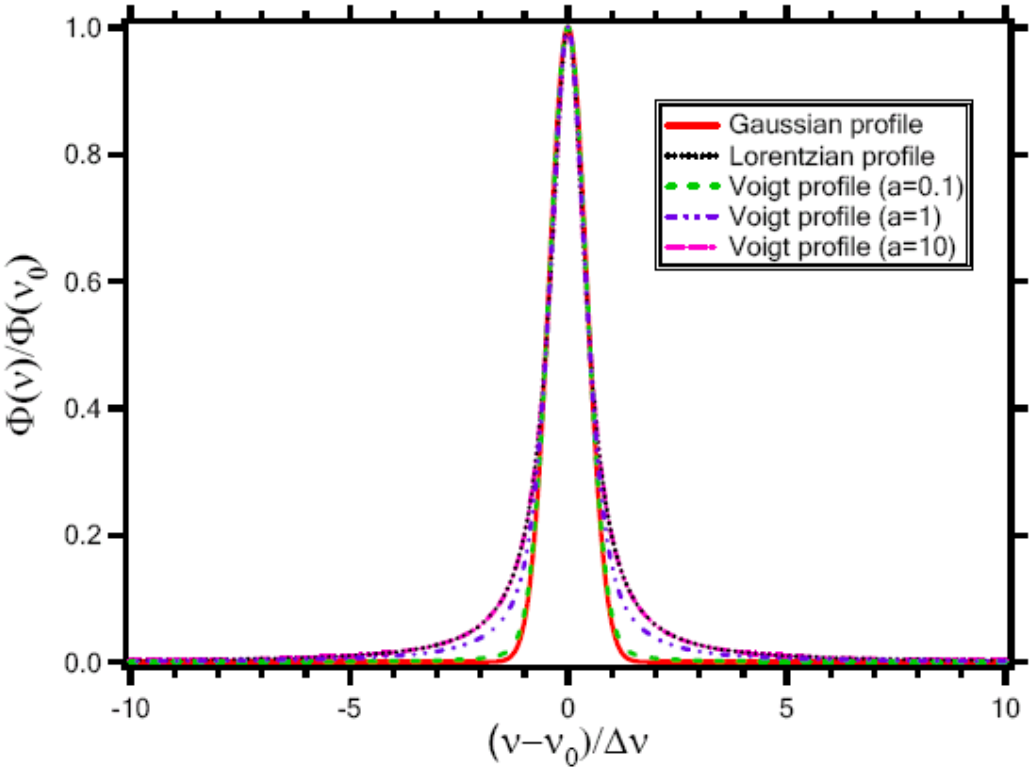

Figure 2.2 - Comparison of Gaussian (Doppler), Lorentzian (collisional), and Voigt (convolution) lineshape profiles [12].

2.4 Measuring Species Concentration and Temperature

Several different methods of laser spectroscopy have been developed. The most common of these options are scanned wavelength direct-absorption, fixed wavelength direct-absorption, and wavelength modulation spectroscopy (WMS). The initial stages (this thesis) of this project only utilize scanned wavelength direct spectroscopy.

2.4.1 Scanned Wavelength Direct Spectroscopy

The most common of the three aforementioned techniques, scanned-wavelength involves "scanning" the laser across a small frequency range which contains the entire transition of interest. In doing so, the complete lineshape is analyzed; enabling the acquisition of several valuable parameters of interest, including temperature and species concentration. Because our setup is well suited to this method, it is what is used for the work of this thesis.

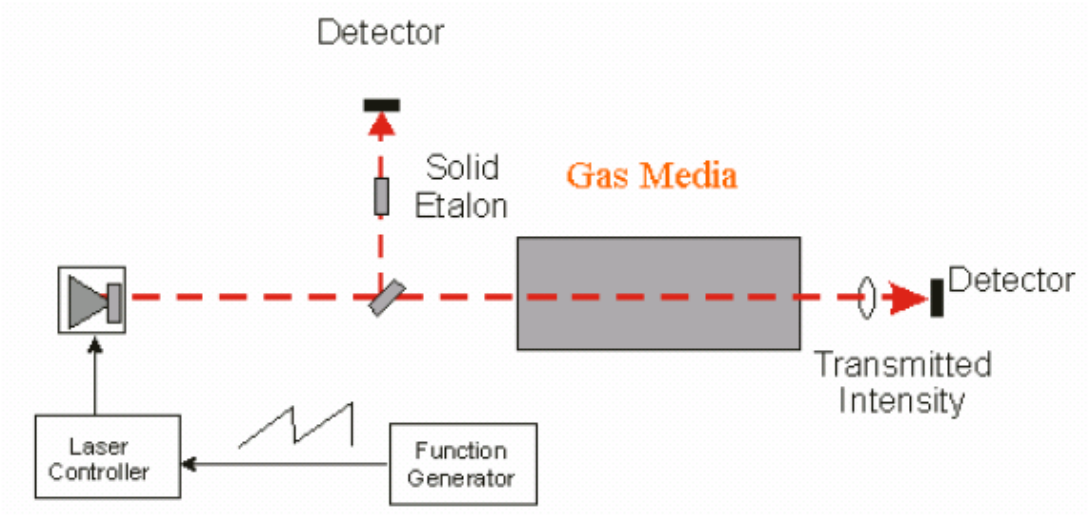

Figure 2.3 - Typical Scanned Wavelength Direct-Spectroscopy Setup [12].

2.4.1.1 Temperature Measurement

Temperature can be obtained in one of two ways when using scanned wavelength. For low pressure situations where Doppler broadening is the dominant mechanism; the Doppler width can be used to quickly assess temperature as follows

$$T = M\left(\frac{\Delta\nu_D}{7.1623x10^{-7}\nu_0}\right)^2$$

where T is temperature, M is the molecular weight of the absorbing species, $\Delta\nu_D$ is Doppler width (FWHM), and ν_0 is line center of the band of interest.

This relation is ineffective at higher pressures due to the dominance of collisional broadening. Thus for higher pressure cases, the so-called 2-line technique is utilized.

The two-line technique compares the linestrength of two different transitions, keeping pressure and path length identical between the two. In doing so, the following ratio between the two scanned transitions can be assessed:

$$R = \frac{A_1}{A_2} = \frac{\int P_{abs} L \phi_{\nu_1} S_1(T) d\nu}{\int P_{abs} L \phi_{\nu_2} S_2(T) d\nu} = \frac{S_1(T)}{S_2(T)} \qquad (2\text{-}1)$$

Linestrength can be expressed as a function of a reference linestrength (at a reference temperature).

$$S_i(T) = S_i(T_0)\frac{Q(T_0)}{Q(T)}\left(\frac{T_0}{T}\right)\exp\left[-\frac{hcE_i^{"}}{k}\left(\frac{1}{T}-\frac{1}{T_0}\right)\right]\left[1-\exp\left(\frac{-hc\nu_{0,i}}{kT}\right)\right]\left[1-\exp\left(\frac{-hc\nu_{0,i}}{kT_0}\right)\right]^{-1}$$

where E" is the lower state energy, k is Boltzmann's constant, c is the speed of light, h is Planck's constant, and Q(T) is the molecular partition function. This partition function is often expressed by the following polynomial, whose coefficients are tabulated in the HITRAN database for various species.

$$Q(T) = a + bT + cT^2 + dT^3$$

If the above relationship is utilized with equation 2-1, the following is obtained

$$\frac{S_1(T)}{S_2(T)} = \frac{S(T_0,\nu_1)}{S(T_0,\nu_2)}\exp\left[-\left(\frac{hc}{k}\right)\left(E_1^{"}-E_2^{"}\right)\left(\frac{1}{T}-\frac{1}{T_0}\right)\right]$$

From which the following temperature expression is obtained

$$T = \frac{\frac{hc}{k}\left(E_2^{"}-E_1^{"}\right)}{\ln\left(\frac{A_1}{A_2}\right)+\ln\frac{S_2(T_0)}{S_1(T_0)}+\frac{hc}{k}\left(\frac{E_2^{"}-E_1^{"}}{T_0}\right)}$$

A_1 and A_2 are the integrated lineshape areas of the two transitions. Selection of transitions is very important when using these relations, as a large difference between the lower energy states of the two lines is desirable for high sensitivity.

2.4.1.2 Species Concentration Measurement

Because the integrated absorbance area is directly proportional to partial pressure, species concentration can easily be obtained with the following relation

$$X = \frac{A}{\int PL\phi_{\nu} S(T) d\nu} = \frac{A}{PLS(T)}$$

where A is integrated absorbance area, P is total pressure, L is path length, and S(T) is linestrength.

3. EXPERIMENTAL METHOD

3.1 Experimental Apparatus

Given that the goal of this project is to develop a diagnostic, developing the experimental apparatus is paramount to this research and thesis. This setup has been evolving over the past several months and will continue to do so as the project moves forward. Currently the system is large, consuming nearly an entire optical table. Ultimately, the goal is to reduce this system into one small unit which can be used in systems such as fuel cells and combustors. The system which was developed for and described in this thesis is illustrated in figure 3.1 below.

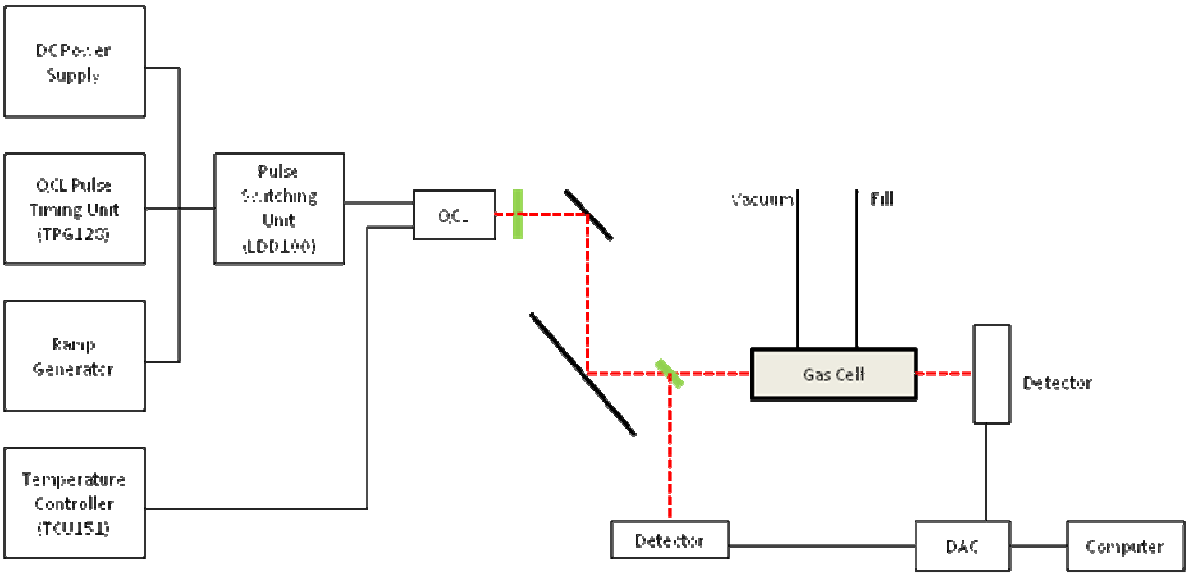

Figure 3.1 – Schematic of diagnostic.

Essentially there are three sections of this setup: laser, beam path, and detector/data collection. QCL (the laser) and all equipment to the left of it are devices which are necessary to the operation of the laser and production of the laser beam. Once the beam leaves the QCL housing, it is collimated and focused by a series of lenses and mirrors. Additionally, the beam is split and one section of the split beam is passed through the gas cell. Finally, these two beams are monitored by two detectors.

3.1.1 Quantum Cascade Laser

To produce the mid-IR beam, a distributed feedback (DFB) quantum cascade laser (QCL) and starter kit manufactured by Alpes Lasers were utilized. A model sb1843 laser diode was used for the CO experiments done here; this particular model produces wavelengths in the range 4569.5 nm – 4590.9 nm (or in wavenumber, 2188.4 cm^{-1} – 2178.2 cm^{-1}).

A quantum cascade laser is a semiconductor diode laser, developed in 1994 by Faist, et al. at AT&T Bell labs [13]. These lasers differ from conventional diode lasers in that rather than emitting across a single band transition (between conduction and valance bands in a doped semiconductor), they are built in a way that causes emission at several sub-bands. These subband emissions are facilitated by the layering of several different semiconductors; as electrons pass across one layer and cause the emission of a photon, they pass to the next layer for the next emission. Figures 3.2 and 3.3 give a graphical illustration as to how a QCL emission pattern differs from that of a conventional semiconductor laser.

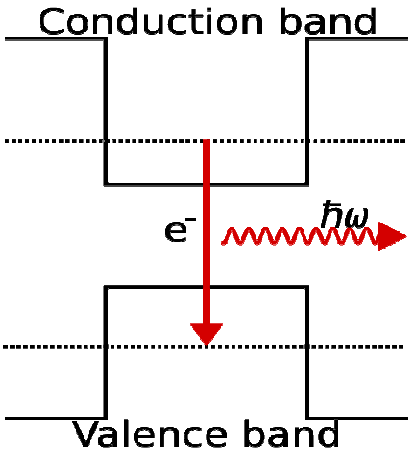

Figure 3.2 – Emission of typical diode.

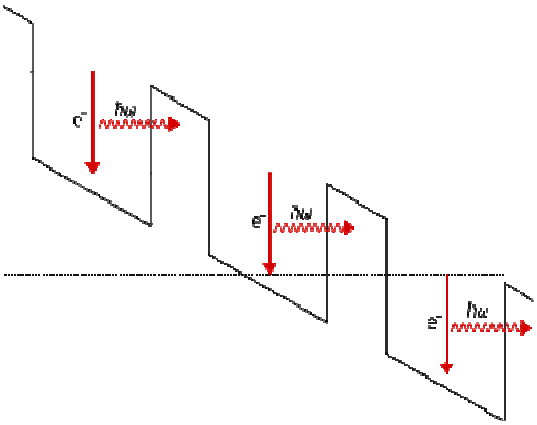

Figure 3.3 – Emission of QCL.

Figure 3.3 shows how a single electron "cascading" down the different band gaps of the layered semiconductor releases multiple photons, giving rise to the quantum *cascade* laser.

A distributed feedback QCL (DFB – QCL) is a specific variant of the laser [14] which utilizes a distributed Bragg reflector (grating) to only allow emission at the desired wavelength. These lasers are tunable largely by temperature; however, it was found that when these DFB-QCLs are pulsed, rapid scanning of a particular wavelength region can be obtained.

This ability to be tuned and rapidly scanned is essential to the scanned-wavelength spectroscopy method discussed in section 2.4.1, which is utilized for this work. Our particular laser built by Alpes lasers consists of a ridge of InGaAs and AlInAs grown on InP with a Fabry-Perot cavity to build up laser oscillation [10].

3.1.2 Laboratory Laser Housing (LLH100)

Proper operation of the laser requires that several conditions be met. Because the laser is a small and fragile semiconductor device, it must be protected from the outside environment, preferably in an inert gas environment, such as Argon. The laser must be kept at a constant particular temperature to produce the desired wavelength and protect the laser from overheating. Also, the laser must obviously be supplied with proper signal to produce emission.

All of these needs are satisfied by a laser housing built by Alpes lasers as part of the starter kit. Within the housing, the laser is mounted on top of a thermoelectric Peltier cooler; this keeps the laser at the desired temperature. Because the Peltier cooler generates a large amount of heat, a water cooling circuit is integrated below the Peltier cooler. A water chiller provides this cooling circuit with 10°C water at approximately 0.25 l/min. Connection to the laser is provided via a low-impedance line which connects directly to the pulser unit (LDD100). The Peltier cooler is connected to a temperature controller (TCU151) which controls the laser temperature to 0.1 °C. Finally, the laser housing offers two LEMO monitoring connections which can be used to monitor the voltage across the laser [10].

3.1.3 Signal Generation Devices

Power provided to the laser is produced by the combined efforts of several devices. Laser pulses are generated by a QCL pulser timing unit (TPG128). This unit provides TTL pulses with duration adjustable between 0 and 200 ns; pulse interval is also adjustable, from 200 ns to 100 μs.

Current pulses generated by the TPG128 are transmitted to the QCL pulse switching unit (LDD100). The LDD100 QCL pulse switching unit is an amplifier/switcher which is based on a MOSFET circuit. The LDD100 amplifies the pulses from the TPG128 and sends them to the laser via a low-impedance ribbon. The LDD100 amplifies the pulses with DC power provided from an adjustable 0-30V power supply. Additionally, the LDD100 can, for scan wavelength operation, combine the amplified current pulses with a more slowly varying subthreshold current provided by an Agilent Technologies function generator. Typically a ramp signal is applied for rapid wavelength scanning (discussed in 3.2.1).

3.1.4 Beam Manipulation

Beam manipulation is a necessary and difficult task associated with this work. Mid-IR radiation obviously cannot be seen by the human eye, and typical sensing materials used with near-IR (such as luminescent paper) do not exist for the mid-IR. Alpes states that the beam diverges off of the laser face approximately 60° in the vertical and 40° in the horizontal. Because of this divergence, beam focusing and collimation is required; to do so, a ZnSe collimating lens from Janos optics is used to first collimate the diverging laser as soon as it leaves the laser housing. After collimation, the laser is focused using a 10 cm and 100 cm focusing mirrors. After focusing, the beam is split using a 10 mm ZnSe flat optic.

In these initial stages of the project it has been difficult aligning the optical train. Thus far, the method has consisted of utilizing an Ophir power meter to measure beam intensity; adjustments are made with each component of the optical system as to maximize measured beam power. This method is rather unsatisfactory as we are blind to the actual beam shape, direction, and divergence. However, it has provided us with a

beam which has been successfully used for initial experiments. Future revisions are proposed in section 4.2.

3.1.5 Gas Cell (Absorbing Media)

For development of the diagnostic system it is necessary to make measurements in a controlled environment. Here we use a heated, stainless steel, 10 cm pathlength gas cell manufactured by International Crystal Laboratories. The cell is constructed from a 10 cm long 3 cm diameter stainless steel tube. Tube ends are closed with CaCl windows (these allow a 90% transmission in the mid-IR) which are vacuum sealed with triple PFTE gaskets. Additionally, the cell has two ports which allow evacuation and gas filling. A heating jacket hugs the exterior of the tube; temperature is measured by a thermocouple which is located at the center of the tube volume.

The current vacuum system (Swagelok plumbing and old single stage belt driven Welch pump) allows the tube to be brought to near vacuum (<1 torr); gas is filled via a set of Swagelok valves and fittings and pressure is measured with a 1000 Torr Baratron pressure manometer. For these experiments gas mixtures were made by diluting a 10% CO/Ar mixture with pure (99.999%) N_2.

3.1.6 Detection and Data Collection

For absorption spectroscopy it is necessary to measure the beam both before and after it passes through the gas sample. To do this, the beam is split as discussed above, the absorbance signal beam is passed through the gas cell and then onto a detector, the other is directed onto a detector from the ZnSe beam splitter located prior to the gas cell.

Detection of the mid-IR laser radiation has been a problem in this project thus far. Since the laser is rapidly scanned via the bias-tee operation (see section 3.2.1) it is necessary to resolve these scans. Additionally, we would like to be able to resolve each individual laser pulse; these are very fast, in the 50 MHz range.

For this thesis, two PDA20H Thorlabs detectors were used. These detectors have a relatively low time response, and are AC coupled, thus unable to detect a constant wavelength pulsed beam. However, they are able to resolve the scanned laser in bias-tee

operation. These detectors are not optimal for this work, and will be replaced soon by much faster HgCdTe detectors when they arrive.

Data is collected by a National Instruments DAC with a labview applet. Our labview applet simply collects input values from both detectors over a certain period of time. Additionally, the transmittance fraction (I/I_o) can be determined by dividing the two signals; a constant is added to both signals to account for the DC signal not observed by the AC coupled detectors. This DC offset is measured by chopping the beam and recording the peak value after chopping and before decay back to zero.

3.2 Experimental Method

The work done for this thesis is aimed at constructing a mid-IR absorption sensor and making initial room temperature demonstration measurements which can in the future be extended to other conditions (temperature, pressure, gas mixtures) and lead to a robust CO sensor for application in a variety of energy systems. These initial experiments involved measurements on $CO/Ar/N_2$ gas samples at known concentration, temperature, and pressure.

Here scanned wavelength direct absorption spectroscopy is performed. This is accomplished by rapidly scanning the laser over a small range of wavelengths in an area where an absorption feature is known to exist. As discussed in section 2, this can resolve an absorption feature; mathematics behind these absorption features can be used to obtain concentrations of the species of interest. At the time of this writing detector time resolution limited our measurements. Also, we do not yet have a way of measuring the variation beam wavelength; this is usually accomplished through the use of an etalon.

Actual operation of the laser is performed by cooling (or heating) the laser to the desired temperature, activating the pulse generator, applying a constant DC voltage, and finally applying a ramp voltage (for bias-tee operation). Wavelength of a QCL is a function of laser temperature and applied voltage. That said, the laser is tuned to a certain wavelength by setting the temperature of the laser via the Peltier cooler, and applying a DC voltage. The literature provided by Alpes Laser gives a chart with estimated output wavelength for temperatures and voltages as seen here in Figure 3.4.

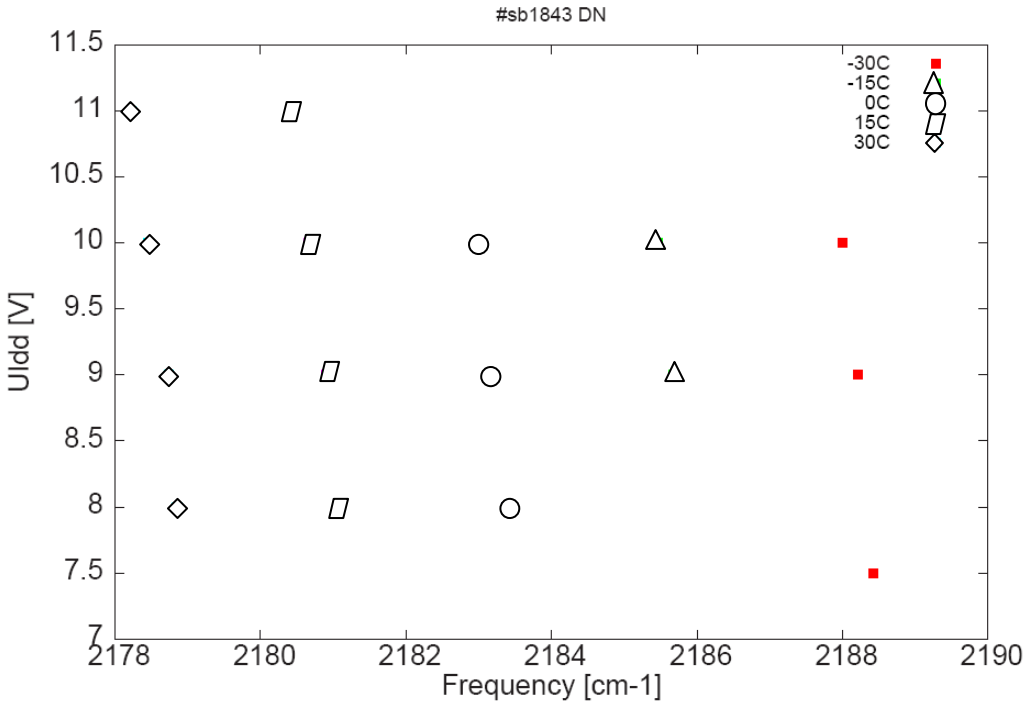

Figure 3.4 – Laser frequency at various settings [10]

While this is useful for approximating the wavelength, it is by no means exact, and actual variation in wavelength must be measured via an etalon.

3.2.1 Bias Tee Operation

Scanning of the laser is accomplished through what is known as "bias tee" operation. In this method, an additional voltage is applied across the laser in the form of a ramp signal. By increasing the voltage across the laser, the temperature of the active region is briefly increased, changing laser wavelength (changing temperature is the primary method of tuning QCL wavelength). According to the laser manufacturer (Alpes Laser), a wavelength shift of 0.1% is achievable using a maximum ramp voltage range of 0 to 3 V.

Ramp frequency is important, as each ramp will potentially capture the spectral feature of interest. While this is not of issue at this phase of the project, eventually the laser will applied to environments which are highly transient, requiring a very fast ramp

frequency to capture the changing spectral response with the variable environment. This again brings up the issue of detectors, as a much faster ramp frequency will require the use of a detector with faster time response to resolve the ramps. For some of the transient environments of interest, scanning rates will need to be on the order of kHz. It has been documented that several operators have utilized scanning rates in the kHz without immediate adverse effects to the laser, however lifetime reduction is expected.

4. EXPERIMENTAL RESULTS

Experimental results for this thesis consist of two majors parts: validation of laser operation, and identification of an absorption feature. Qualitative measurements are approximate at best, more importantly is the appearance and identification of absorbance features in an environment with CO.

4.1 Validation of Laser Operation

Once the laser setup was completed, the first objective was to validate proper operation of the laser. This was accomplished through the use of a model 3A laser power meter from Ophir optics. The laser manufacturer provides a specification sheet for the laser, including data for applied voltage vs. power output. With this information, we collected power measurements at the same conditions (temperature and applied voltage) to produce a similar power curve graph. Here figures 4.1 and 4.2 compare the manufacturer's specifications and our own measurements, respectively.

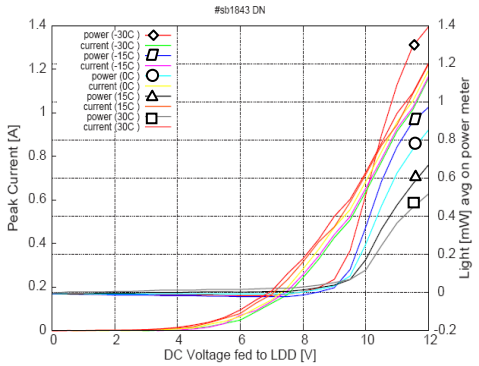

Figure 4.1 Output current and power [10].

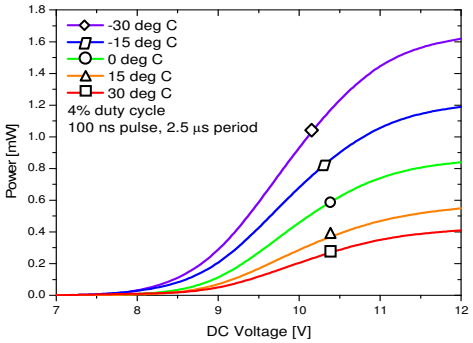

Figure 4.2 – Measured power.

There is generally good agreement between our measured values for laser output and the manufacturer's measurements. The manufacturer custom builds each laser, thus the data supplied on the specification sheet is measured from the actual laser being supplied. That said, agreement should be very close, as it is here, well within reason of variables such as differences in curve fitting and precision in data collection.

4.2 Initial Measurements

After laser functionality was confirmed, several initial experiments were performed to demonstrate the ability to detect spectral features of CO. These experiments consisted of filling the gas cell with several different mixtures of CO and N_2 with varying concentrations of CO.

We were able to identify the CO R(11) absorption feature, centered at the wavenumber 2186.6 cm^{-1} (4.57 μm wavelength). By setting the laser to -25°C, and applying a constant DC voltage of 10.2 V, we were able to get in the general vicinity of this feature. A ramp voltage which ramped from 600 mV to 2 V was applied at 20 Hz via bias tee, facilitating scanning across the spectral feature.

Four different gas mixtures were measured: a baseline with the cell at near vacuum (<1 torr), and three runs at atmospheric pressure, CO partial pressures of 2.5, 5, and 10 torr, with balance N_2. The same spectral feature was noticed at each different concentration of CO; increasing intensity was noticed with increasing CO concentration, as expected.

Demonstrating our ability to see and identify a feature being the main goal here, the 2.5 torr CO vs. vacuum baseline is used as an illustrative example. In this case, a partial pressure of 2.5 CO/Ar mixture was added to the cell (this is a 10% CO, 90% Ar mixture). Cell pressure was brought to 743.6 torr with the addition of N_2. With temperature held constant at approximately 298 K, CO concentration of 336 ppm is achieved through this mixture.

With the above laser settings and gas mixture characteristics, the following data was collected. Figure 4.3 illustrates the time response of detector located after the cell for both the baseline vaccum case and 336 ppm CO case.

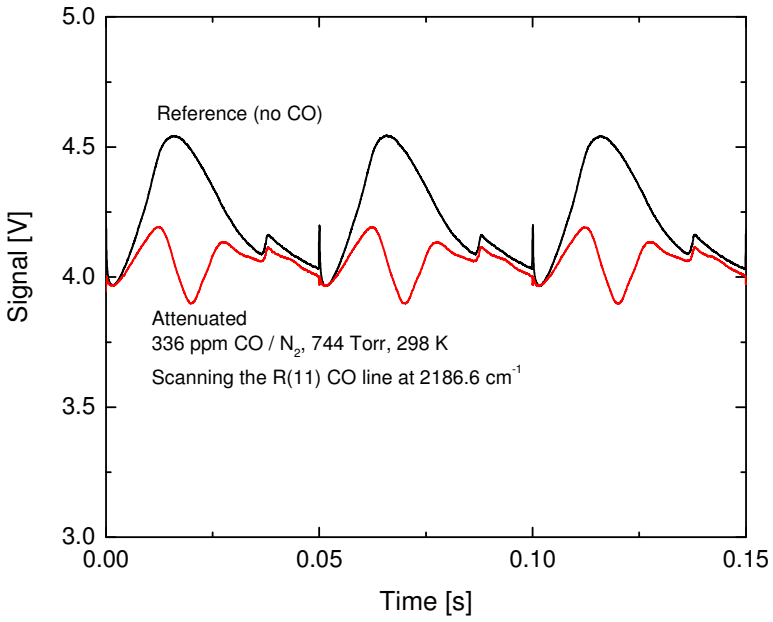

Figure 4.3 – Time response of detector with baseline and 336 ppm CO case.

Figure 4.3 illustrates several interesting features. As it is a time dependent graph, the ramp effect can be seen in the form of detector signal peaks. More importantly, the R(11) CO absorbance line can be clearly identified as the significant dip in the attenuated signal when compared to the baseline reference signal. The region of overlaps in the two signals indicates regions where there is no absorbance.

To confirm that this is a spectral feature, and indeed the R(11) absorbance line, data was compared to the result obtained from the HITRAN database [15]. Using the mathematical relations explained in section 2, a MATLAB code is used to produce the Voigt profile of the R(11) feature at our temperature and concentration using data from the HITRAN database. Plotting versus frequency required the fitting of our timebased data to a frequency domain; this was accomplished using manufacturer specifications for frequency vs. subthreshold voltage (this is a function of applied voltage and ramp voltage). Additionally, the MATLAB code produces a plot of absorbance (k_vL) therefore absorbance was calculated by taking the natural logarithm of the 336 ppm CO divided by the baseline signals, show in the following expression.

$$(k_v L) = \ln\left(\frac{I_{CO}}{I_{baseline}}\right)$$

Some skewing of the line occurs as a result of this fit, however the agreement shown in figure 4.4 between data and HITRAN/theory is quite good considering this was a preliminary run.

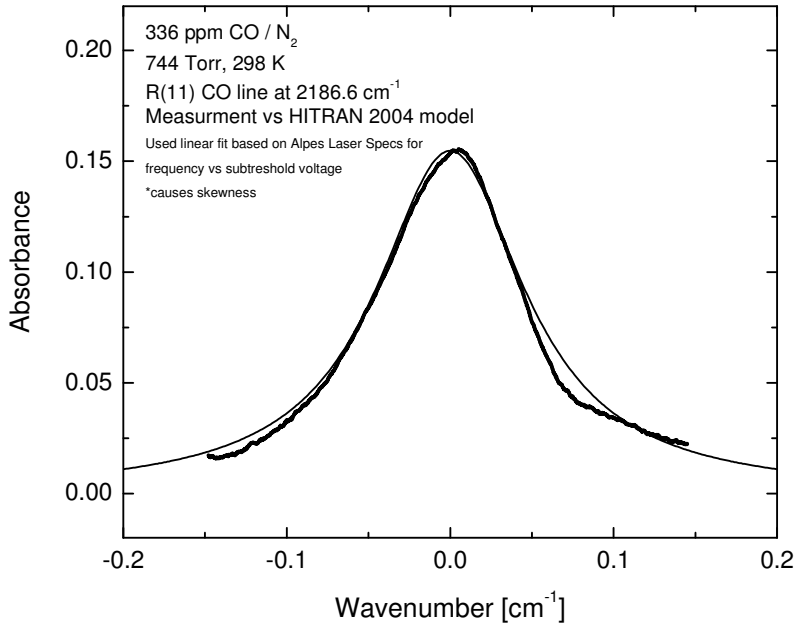

Figure 4.4 - Comparison of HITRAN to observed absorbance.

Again, this experiment was repeated for two more concentrations of CO with partial pressures of 5, 10, and 20 torr, corresponding to CO mole fractions of approximately 800 ppm, 1600 ppm, and 3800 ppm, respectively. Peak absorbance for each was calculated and plotted against the absorbance predicted by HITRAN. Measured peak absorbance and HITRAN expected absorbance are shown as black squares and a black line, respectively in figure 4.5.

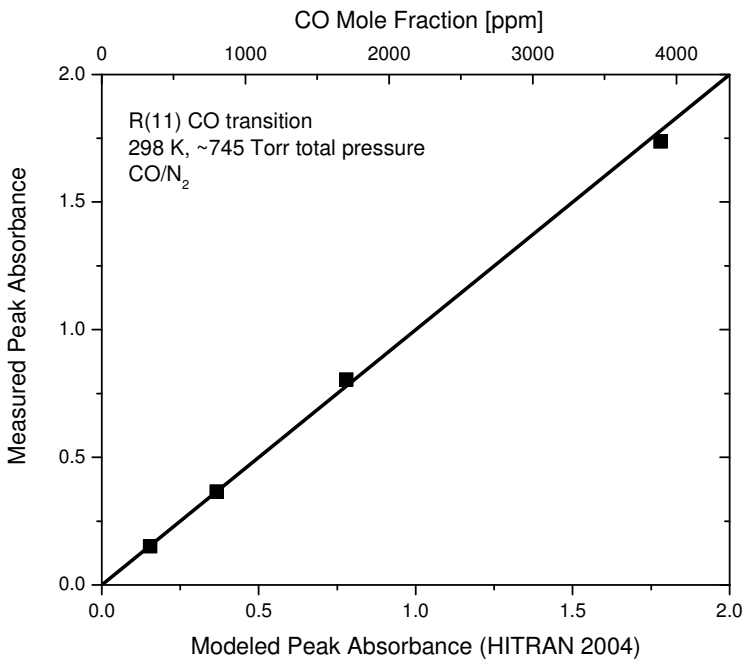

Figure 4.5 - Measured and HITRAN absorbances for different CO concentrations.

As expected, peak absorbance rises with increasing CO concentration. Additionally, measured absorbance is very close to that predicted by the HITRAN 2004 model.

5. DISCUSSION AND CONCLUSIONS

Previous work with mid-IR spectroscopy using quantum cascade lasers is limited. Almost all of the work done thus far in this area has dealt with measurements of steady state controlled environment gas samples. While this thesis deals only with the "simple" steady state, controlled scenario, it has demonstrated the difficulty of such work.

5.1 Achievements

While the work of this thesis represents a small step in the process of developing the diagnostic envisioned in the main goals of the project [1], a great deal of groundwork has been laid for the future. Much was learned about the operation of quantum cascade lasers, as well their use in spectroscopy applications. Challenges were encountered throughout the work; given the limited use of these devices, there was little to reference along the way.

Initial stages dealt with learning how to operate the laser. A general lack of literature and communication difficulties with the manufacturer (based in Switzerland) led to the overheating, overvoltage, and subsequent destruction of the first laser (model sb616). From this we learned several things, the requirement of water cooling and maximum acceptable voltages. Additionally, in the process of diagnosing laser problems we were able to gain a much better understand about how the laser functions and interacts with the other components of the system; the value of this knowledge may be invaluable in dealing with future problems which may arise.

Once the system was finally made operational, we were able to validate correct operation of the laser, as well as make some preliminary measurements. These early data allowed us to successfully see and identify the R(11) CO spectral feature, proving the capability of our system to see the absorption features of CO in the mid-IR using a quantum cascade laser. While quantitative measurements were not yet possible with our current detectors, the ability to find and identify a spectral feature in the correct location (with respect to wavelength) was a critical step forward for the project.

5.2 Future Work

Accomplishments made in the work covered by this thesis represent only a small portion of the desired work of this project as a whole. The ultimate goal of this project is develop laser sensors for not only CO, but H_2O, and CO_2 as well.

Of immediate concern is finding and implementing new detectors which have a much faster time response than the current detectors, allowing resolution of the laser pulse and capture of the peak laser intensity. This will greatly aid in lower noise measurements for very small concentrations of carbon monoxide.

Also of concern in the near future is finding ways to better align the optical train. As mentioned in section 3.1.4, beam collimation, focusing, and alignment has been marginal at best. Several ideas have been suggested for better beam alignment, such as the addition of a visible laser beam to the IR beam, or more precise planning of the optical train. Regardless, for optimal beam usage and more accurate measurements, this is a significant consideration. Additionally, a method of quantifying wavelength variation must be considered, either through an etalon or some other means.

Once these new detectors (HgCdTe) are obtained and brought online, the diagnostic as constructed for this work should provide highly sensitive CO measurements. The next step will be to continue validation of the laser by making gas cell measurements at different temperatures and pressures. Following cell measurements, plans are to apply the laser to the low pressure shock tube in the RPI combustion lab. Initial shock tube measurements will be aimed at high-temperature constant CO concentration environments, for validation of the sensor at extreme conditions. Following validation, the sensor will be applied to transient shock tube environments such as hydrocarbon oxidation and ignition and in the future the hope is to apply the sensor to a range of combustion and energy systems such as flames, fuel cells, gasifiers, reformers, etc.

6. REFERENCES

[1] Oehlschlaeger, M.A., 2007, "Mid-Infrared Laser Absorption Diagnostics for Characterization, Monitoring, and Control of Combustion and Fuel Cell Power Generation and Propulsion Devices", A Proposal for Research to the Office of Naval Research Young Investigator Program.

[2] F.K. Tittel, Y. Bakhirkin, A.A. Kosterev, and G. Wysocki, "Recent Advances in Trace Gas Detection Using Quantum and Interband Cascade Lasers," *The Review of Laser Engineering* 34, 275-282 (2006).

[3] D. Weidmann, F.K. Tittel, T. Aellen, M. Beck, D. Hofstetter, J. Faist, and S. Blaser, "Mid-Infrared Trace-Gas Sensing with a Quansi-Continuous-Wave Peltier-Cooled Distributed Feedback Quantum Cascade laser," *Applied Physics B* 79, 907-913 (2004).

[4] G. Wyscoki, A.A. Kosterev, and F.K. Tittel, "Spectroscopic Trace-Gas Sensor with Rapidly Scanned Wavelengths of a Pulsed Quantum Cascade Laser for In Situ NO Monitoring of Industrial Exhaust Systems," *Applied Physics B* 80, 617-625 (2005).

[5] C. Roller, K. Namjou, J.D. Jeffers, M. Camp, A. Mock, P.J. McCann, and J. Grego, "Nitric Oxide Breath Testing by Tunable-Diode Laser Absorption Spectroscopy: Application in Monitoring Respiratory Inflammation," *Applied Optics* 41, 6018-6029 (2002).

[6] B.A. Paldus, C.C. Harb, T.G. Spence, R.N. Zare, C. Gmachl, F. Capasso, D.L. Sivco, J.N. Baillargeon, A.L. Hutchinson, and A.Y. Cho, "Cavity Ringdown Spectroscopy Using Mid-Infrared Quantum-Cascade Lasers," *Optics Letters* 25, 666-668 (2000).

[7] Q. Shi, D.D. Nelson, J.B. McManus, M.S. Zahniser, M.E. Parrish, R.E. Baren, K.H. Shafer, and C.N. Harward, "Quantum Cascade Infrared Laser Spectroscopy for Real-Time Cigarette Smoke Analysis," *Analytical Chemistry* 75, 5180-5190 (2003).

[8] K. Namjou, S. Cai, E.A. Whittaker, J. Faist, C. Gmachl, F. Capasso, D.L. Sivco, and A.Y. Cho, "Sensitive Absorption Spectroscopy with a Room-Tempreature Distributed-Feedback Quantum-Cascade Laser," *Optics Letters* 23, 219-221 (1998).

[9] S. Wehe, D. Sonnenfroh, M. Allen, C. Gmachl, and F. Capasso, "Quantum-Cascade Laser-Based Sensor for CO and NO Measurements in Combustor Exhaust Flows," *37th AIAA/ASME/SAE/ASEE Joint Propulsion Conference* (2001).

[10] Alpes Lasers, "Quantum Cascade Laser Starter Kit Instructions Manual", Version 3.1 02.07. Alpes Lasers SA, 1-3 Passage Max-Meuron CP 1766 CH-2001 Neuchatel, Switzerland. Tel ++41 32 7299510 http://www.alpeslasers.ch

[11] Webber, M. E., 2001, Diode Laser Measurements of NH_3 and CO_2 for Combustion and Bioreactor Applications. (Doctoral Dissertation, Stanford University, January 2001). *Stanford University Thermosciences Department.*

[12] Zhao, X., 2005, Diode-Laser Absorption Sensors for Combustion Control. (Doctoral Dissertation, Stanford University, July 2005). *Stanford University*

Thermosciences Department.

[13] Faist, J., Capasso, F., Sivco, D. L., Sirtori, C., Hutchinson, A. L., Cho, A. Y., 1994, "Quantum Cascade Laser", *Science*, vol. 264, pp. 553-556.

[14] Faist, J., Gmachl, C., Capasso, F., Sitori, C., Sivco, D. L., Baillargeon, J. N., Cho, A., 1997, "Distributed Feedback Quantum Cascade Lasers", *Applied Physics Letters,* vol. 70, issue 20, pp. 2670-2672.

[15] L. S. Rothman, D. Jacquemart, A. Barbe, D. Chris Benner, M. Birk, L. R. Brown,M. R. Carleer, C. Chackerian Jr., K. Chance, L. H. Coudert, V. Dana, V. M. Devi, J.-M. Flaud, R. R. Gamache, A. Goldman, J.-M. Hartmann, K. W. Jucks, A. G. Maki, J.-Y. Mandin, S. T. Massie, J. Orphal, A. Perrin, C. P. Rinsland, M. A. H. Smith, J. Tennyson, R. N. Tolchenov, R. A. Toth, J. Vander Auwera, P. Varanasi, and G. Wagner, "The HITRAN 2004 Molecular Spectroscopic Database," *Journal of Quantitative Spectroscopy and Radiative Transfer* 96, 139-204 (2005).